COMPUTER METHODS AND PROGRAMS IN BIOMEDICINE 112 (2013) 398–406

journal homepage: www.intl.elsevierhealth.com/journals/cmpb

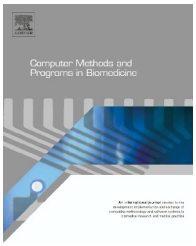

A Gauss–Newton approach to joint image registration and intensity correction

Mehran Ebrahimi[a,*], *Anthony Lausch*[b], *Anne L. Martel*[c]

[a] *Faculty of Science, University of Ontario Institute of Technology, 2000 Simcoe Street North, Oshawa, Ontario, Canada L1H 7K4*

[b] *Department of Medical Biophysics, University of Western Ontario, London Regional Cancer Program, 790 Commissioners Road East, London, Ontario, Canada N6A4L6*

[c] *Department of Medical Biophysics, University of Toronto Imaging Research, Sunnybrook Research Institute, 2075 Bayview Avenue, Toronto, Ontario, Canada M4N 3M5*

ARTICLE INFO

Article history:
Received 17 July 2012
Received in revised form
29 July 2013
Accepted 30 July 2013

Keywords:
Image registration
Inverse problems
Intensity correction
Optimization
Multi-level

ABSTRACT

We develop a new efficient numerical methodology for automated simultaneous registration and intensity correction of images. The approach separates the intensity correction term from the images being registered in a regularized expression. Our formulation is consistent with the existing non-parametric image registration techniques, however, an extra additive intensity correction term is carried throughout. An objective functional is formed for which the corresponding Hessian and Jacobian is computed and employed in a multi-level Gauss–Newton minimization approach. In this paper, our experiments are based on elastic regularization on the transformation and total variation on the intensity correction. Validations on dynamic contrast enhanced MR abdominal images for both real and simulated data verified the efficacy of the model.

The pursued approach is flexible in which we can exploit various forms of regularization on the transformation and the intensity correction.

1. Introduction

The goal of this paper is to develop a new efficient numerical methodology for automated simultaneous registration and intensity correction of images [2,8,13,29,34–36]. A key ingredient and the main novelty of the new approach is the integration of intensity change compensation and motion correction into a unified mathematical model. Rather than dividing the task into two sub-problems and to treat these sub-problems sequentially and independently, the new approach assumes that these sub-problems are in fact related and mutually dependent. This paper is therefore based on a generalized variational framework, which integrates changes of positions and changes of intensities into a combined optimization framework.

Motion correction is typically based on an alignment strategy, which aims to establish correspondences between related points in different images. The technique for the alignment of images taken at different times, from different perspectives, or from different devices is known as image registration, fusion, or warping. As motion provides one of the key challenges in medical imaging, it is no surprise that an overwhelming number of publications address this issue; see, e.g., the books [21,40,32,51,15,42,33] the overview articles [5,14,27,39,24,53,10], and references therein. Although

* *Corresponding author*. Tel.: +1 905 721 8668x6236.
E-mail address: mehran.ebrahimi@uoit.ca (M. Ebrahimi).

0169-2607/$ – see front matter © 2013 Elsevier Ireland Ltd. All rights reserved.
http://dx.doi.org/10.1016/j.cmpb.2013.07.026

the alignment problem is essential for the treatment of many imaging applications its solution is far from being trivial.

For example, the registration problem in dynamic contrast enhanced magnetic resonance imaging (DCE-MRI) presents a particular challenge as intensity changes at a certain location can be based on motion, contrast agent uptake, or both. In contrast to other applications, where intensity variation might be modelled as noise, intensity variation in DCE-MRI is signal and thus requires an appropriate treatment. Existing distance measures either assume time homogeneity of spatial intensity variations and are thus inappropriate or are feature based and thus too restrictive. In this context, several authors have proposed a dual approach where the first step is to estimate the intensity-enhancement and the second step is to align the images after compensating for the intensity changes. Examples of this approach is given in [52,26] where the intensity variation in the template image is estimated first and then this information is used to "de-enhance" the template image. Once this is done, the transformation between the template and the reference images is calculated. This process is repeated in an iterative fashion until convergence occurs. In [6] a pharmacokinetic model is fitted to the data and this is used to estimate the intensity enhancement for each voxel; the template image is then registered to a synthetic image which is generated by adding the expected intensity enhancement to the pre-contrast reference image. Similarly, in [31] a principal components analysis is used to estimate a synthetic sequence of motion free contrast enhanced-images from the original data; each moving image is then registered to the synthetic image from the corresponding time point. All of these approaches have the problem that they attempt to estimate motion and intensity enhancement separately and iterate between the two tasks in the hope that convergence will occur. The limitation of these approaches is that a problem with two mutually dependent components is addressed by sequentially looking at the components. A major challenge in DCE-MRI is to provide a unified framework, that enables a simultaneous treatment for both motion correction and intensity homogenization and thus provides the basis for a proper, robust, and efficient numerical treatment.

Following Horn-Schunck's seminal work [25] on estimating the motion using optical flow, a number of approaches were proposed in the literature [13,36,50] which allowed varying illumination among the two images being registered. The approaches developed in [13,36] were very similar to Horn-Schunck's, except that they separated the illumination change as a linear intensity shift term. More recently, a similar idea was applied to the registration of contrast-enhanced images [2,29]. This allowed intensity correction along with registration which is not directly provided by sophisticated registration distance measures. The common intuition behind these methods was separating and regularizing the intensity correction term from the images in the regularization expression coupled with the motion. Numerically, these approaches proposed constructing a very large system of equations directly based on the slightly modified optical flow equations. Iterative solvers were then used to minimize the objective functional and estimate the deformation vectors. All of these methods used the diffusion penalty [32] function on the displacement field, however, the possibility of applying other regularization expressions was not readily available.

A model we have developed in this direction [9] suggests a variant of the well known Demons algorithm [45]. Although the original Demons model does not allow any change of the intensity in images to be registered, we allow intensity changes in the proposed model. Although the approach is promising and yields a generalization of the Demons algorithm, a precise mathematical explanation of the model seems to be a challenge, and the arbitrary choice of the smoothing kernels and their various associated parameters seem to be rather challenging. The methods in [8,34,35] also tend to unify and generalize the intensity correction and registration. Recently in [8], we presented a general PDE-framework for registration of contrast enhanced images. Furthermore, [34,35] model the intensity correction as a multiplicative term. However, this is not sufficient because loosely speaking if the intensity of a pixel is zero in one image and non-zero in the other one, a multiplicative intensity correction factor cannot fix this. In our proposed scheme in this manuscript our model is similar to [8], except that a more generalized regularization expression is employed. Furthermore, the more efficient Gauss–Newton approach in a multi-level implementation [37,33] is used as opposed to the steepest descent method in [8]. In addition, we perform preliminary validation experiments on real and simulated data.

In Section 2, we will introduce the mathematical formulation and problem set-up. In Section 3, we will focus on the discretization of the described problem. The derivation of a numerical scheme and simple computational experiments will be followed in Sections 4 and 5. Finally, we will present validations and concluding remarks in Sections 6 and 7.

2. Mathematical formulation

Consider the registration problem of a template image $\mathcal{T}$ to a reference image $\mathcal{R}$, where $\mathcal{T}$ is a realization of $\mathcal{R}$ deformed via a transformation y and the intensity of this realization is changed via an extra additive [image] term w. For consistency, we adopt our notations from [33].

In this paper, the d-dimensional reference and template images are represented by mappings $\mathcal{R}, \mathcal{T}: \Omega \subset \mathbb{R}^d \to \mathbb{R}$ of compact support. The goal is to find the transformation $y : \mathbb{R}^d \to \mathbb{R}^d$ and a compactly supported intensity correction image $w : \Omega \subset \mathbb{R}^d \to \mathbb{R}$ such that $\mathcal{T}[y] + w$ is similar to $\mathcal{R}$, in which $\mathcal{T}[y]$ is the transformed template image and $\mathcal{T}[y] + w$ is the intensity-corrected deformed image. We formulate joint image registration and intensity correction of a template image $\mathcal{T}$ to a reference image $\mathcal{R}$ as following.

Problem 1. Given two images $\mathcal{R}, \mathcal{T}: \Omega \subset \mathbb{R}^d \to \mathbb{R}$, find a transformation $y : \mathbb{R}^d \to \mathbb{R}^d$ and an intensity correction image $w : \Omega \subset \mathbb{R}^d \to \mathbb{R}$ that minimize the joint objective functional

$$\mathcal{J}[y; w] := \mathcal{D}[\mathcal{T}[y] + w, \mathcal{R}] + \alpha\mathcal{S}[y - y^{\text{ref}}] + \beta\mathcal{Q}[w]. \tag{1}$$

Here, $\mathcal{D}$ measures the dissimilarity of $\mathcal{T}[y] + w$ and $\mathcal{R}$, and $\alpha\mathcal{S} + \beta\mathcal{Q}$ is a regularization expression on $[y; w]$. It is assumed that $y^{\text{ref}}(x) = x$. Furthermore, sum of squared distances (SSD) is

used as the dissimilarity measure, the elastic regularization is applied to the transformation [32,33], and the total variation (TV) [41,49] penalty is used on the additive intensity correction image. Note that TV does not require the contrast modulation to be differentiable and therefore provides an exciting option to model abrupt changes. All of this can be summarized as

$$\begin{aligned}\mathcal{D}[\mathcal{T}+w,\mathcal{R}] &= \mathcal{D}^{\mathrm{SSD}}[\mathcal{T}+w,\mathcal{R}] \\ &= \frac{1}{2}\int_{\Omega}(\mathcal{T}(x)+w(x)-\mathcal{R}(x))^2dx, \end{aligned} \tag{2}$$

$$\mathcal{S}[y] = \frac{1}{2}\int_{\Omega}\mu\langle\nabla y,\nabla y\rangle+(\lambda+\mu)(\nabla\cdot y)^2dx, \tag{3}$$

$$\begin{aligned}\mathcal{Q}[w] = \mathcal{TV}_{\epsilon}[w] &= \int_{\Omega}\sqrt{\|\nabla w(x)\|^2+\epsilon}dx \\ &\approx \int_{\Omega}\|\nabla w(x)\|dx. \end{aligned} \tag{4}$$

3. Discretization

Here we employ a discretize-then-optimize paradigm, (see [18–20,33] and the FAIR software [33] for details) to minimize the functional in Eq. (1). Let $\mathtt{x}$ denote a discretization of the Ω, $\mathtt{y}\approx y(\mathtt{x})$, $w\approx w(P\cdot\mathtt{x})$, $R\approx\mathcal{R}(P\cdot\mathtt{x})$, and $T\approx\mathcal{T}(P\cdot\mathtt{x})$, each corresponding to a discretization as denoted and take $\mathtt{yRef}=\mathtt{x}$. The discretization of the problem is now to minimize the discretized functional

$$J[y;w] := D[T(P\cdot y)]+w,R]+\alpha S(y-yRef)+\beta Q(w). \tag{5}$$

In this expression, the grid interpolation operator $\mathtt{P}$ transfers the problem discretization to cell-centers, see [33]. Discretization of the operators $\mathcal{D}$ and $\mathcal{S}$ are represented by D and S. In addition, the discretization of Total Variation operator $\mathcal{Q}=\mathcal{TV}_{\epsilon}$ is denoted by Q, see [33,49]. Throughout this paper, it is assumed that d-dimensional cell-centered-discretized images R, T each contains n pixels (voxels) and the discretization of the problem, $\mathtt{x}$, contains m pixels (voxels). Table 1 summarizes size

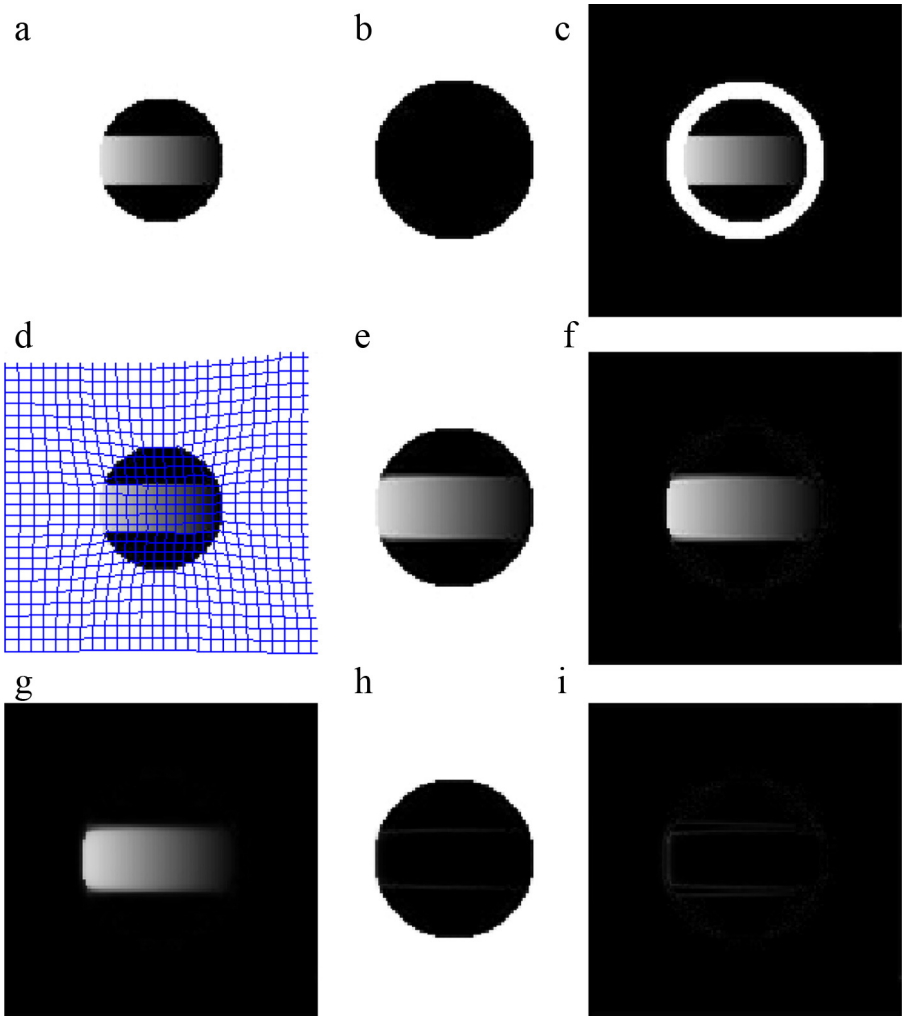

Fig. 1 – Multi-level Gauss–Newton approach to joint image registration and intensity correction of a disk example for level 7: (a) Template $T(\mathtt{x})$. (b) Reference $R(\mathtt{x})$. (c) $|T(\mathtt{x})-R(\mathtt{x})|$. (d) Template $T(\mathtt{x})$ and the grid $\mathtt{y}$ (e) Transformed template $T(\mathtt{y})$. (f) $|T(\mathtt{y})-R(\mathtt{x})|$. (g) Intensity correction $|\mathtt{w}(\mathtt{x})|$. (h) $T(\mathtt{y})+\mathtt{w}(\mathtt{x})$. (i) $|T(\mathtt{y})+\mathtt{w}(\mathtt{x})-R(\mathtt{x})|$.

Table 1 – Size of the matrices

Variable(s)	Size
R, T, w, r	$n \times 1$
x, y	$m \times 1$ [$m = nd$ if centered-grid is used.]
P	$nd \times m$
dT	$n \times nd$
S, Q, J	1×1
dS	$1 \times m$
dQ	$1 \times n$
dJ	$1 \times (m+n)$
H_S	$m \times m$
H_Q	$n \times n$
H_J	$(m+n) \times (m+n)$

of the corresponding matrices throughout this manuscript some of which will be introduced later on.

4. Gauss–Newton approach

We need to compute the Jacobian and Hessian of J denoted by dJ and H_J, respectively in a Gauss–Newton approach described in Algorithm 1 [37].

Algorithm 1. Minimizing $J[\mathrm{y};\mathrm{w}]$ using Gauss–Newton approach

Initialize $\begin{bmatrix} y \\ w \end{bmatrix} \leftarrow \begin{bmatrix} y_0 \\ w_0 \end{bmatrix}$.

while not converged **do**

Evaluate H_J and dJ at $[\mathrm{y};\mathrm{w}]$.

Solve the descent direction from the linear equation $H_J \begin{bmatrix} \delta y \\ \delta w \end{bmatrix} = -dJ^T$.

Find a positive scalar step-size s using a line-search scheme.

Update $\begin{bmatrix} y \\ w \end{bmatrix} \leftarrow \begin{bmatrix} y \\ w \end{bmatrix} + s \begin{bmatrix} \delta y \\ \delta w \end{bmatrix}$.

end while

Note that the Hessian and Jacobian of the regularization S is defined respectively as dS and H_S. Furthermore, we can compute the Hessian and Jacobian of the discretized TV operator denoted by dQ and H_Q respectively. To proceed, the Jacobian of the objective function J can be computed as

$$dJ = \left[\frac{\partial J}{\partial y}, \frac{\partial J}{\partial w}\right]. \tag{6}$$

Now take

$$r = T(P \cdot y) + w - R. \tag{7}$$

Choosing the SSD distance measure and defining

$$\Psi(r) = \frac{1}{2} r^T r \tag{8}$$

yields $\Psi(r) = D[T(\mathrm{P} \cdot \mathrm{y})] + \mathrm{w}, R]$. Hence using the chain-rule

$$\begin{aligned} \frac{\partial J}{\partial y} &= \frac{\partial \Psi}{\partial r}\frac{\partial r}{\partial T}\frac{\partial T}{\partial (P.y)}\frac{\partial (P.y)}{\partial y} + \alpha \frac{\partial S}{\partial y} \\ &= r^T I_n dT\, P + \alpha \frac{\partial S}{\partial y} = r^T dT\, P + \alpha dS, \end{aligned} \tag{9}$$

in which dT represents the derivative of the interpolant available in FAIR [33]. Also,

$$\frac{\partial J}{\partial w} = \frac{\partial \Psi}{\partial r}\frac{\partial r}{\partial w} + \beta \frac{\partial Q}{\partial w} = r^T + \beta \frac{\partial Q}{\partial w} = r^T + \beta dQ. \tag{10}$$

Therefore,

$$dJ = [r^T dT\, P + \alpha\, dS, r^T + \beta\, dQ]. \tag{11}$$

Finally, to compute the Hessian of J denoted by H_J, note that

$$\begin{aligned} dr &= \left[\frac{\partial r}{\partial y}, \frac{\partial r}{\partial w}\right] = \left[\frac{\partial r}{\partial T}\frac{\partial T}{\partial (P.y)}\frac{(P.y)}{\partial y}, \frac{\partial r}{\partial w}\right] \\ &= [I_n dT\, P, I_n] = [dTP, I_n]. \end{aligned} \tag{12}$$

Therefore,

$$\begin{aligned} H_J &= d^2\Psi + \alpha\, d^2_{[y,w]} S + \beta\, d^2_{[y,w]} Q \\ &= dr^T dr + \alpha\, d^2_{[y,w]} S + \beta\, d^2_{[y,w]} Q \\ &= [dT\, P, I_n]^T [dT\, P, I_n] \\ &+ \left[\begin{array}{c|c} \alpha H_S & 0_{m\times n} \\ \hline 0_{n\times m} & \beta H_Q \end{array}\right] \\ &= \left[\begin{array}{c|c} (dT\, P)^T dT\, P + \alpha H_S & (dT\, P)^T \\ \hline dT\, P & I_n + \beta H_Q \end{array}\right]. \end{aligned} \tag{13}$$

Note that the evaluated Jacobian and Hessian of the objective functional J in Eqs. (11) and (13) can now be used in the Gauss–Newton Algorithm 1. For practical implementations of the Hessian and Jacobian of the regularizer and the TV operators see for example [33,49]. We also consider different discrete representations of the joint image registration/intensity correction problem, and address the discrete problems sequentially in the so-called multi-level approach. Starting with the coarsest and thus inexpensive problem, a solution is computed, which then serves as a starting guess for the next finer discretization. This can be written as a sequence of discretizations

$$J^h[y^h; w^h] := D^h[T^h(P^h \cdot y^h)] + w^h, R^h] + \alpha S^h(y^h - \mathrm{yRef}^h) + \beta Q^h(w^h), \tag{14}$$

in which h controls the spatial size of each discretization, see [33]. This procedure has several advantages. It adds additional regularization to the registration problem (more weight is given to more important structure), it is very efficient (typically, most of the work is done on the computationally inexpensive coarse representations, and only a refinement is required on the costly finest representation), it preserves the optimization character of the problem and thus allows the use of established schemes for line searches and stopping. The use of this technique leads to optimal schemes in the sense that only a fixed number of arithmetic operations is expected for every data point.

5. Computational experiments

In the first experiment, we create a toy example similar to the one in [35]. The reference image in this experiment is a disk Fig. 1(b), and the template image a smaller disk with a grayscale ramp on its interior Fig. 1(a). With the multi-level Gauss–Newton approach, we are not only able to compute a reasonable displacement field Fig. 1(d) but also an intensity correction term displayed in Fig. 1(g). Due to this intensity correction term we are now enabled to display the final registered and intensity corrected image $T(yc) + w(xc)$, which in this example happens to be a perfect copy of the reference. In this experiment we used the main parameters $\alpha = 1000$, $\beta = 20$, $\epsilon = 10$, $\mu = 1$, and $\lambda = 0$, along with an Armijo line search [37] and a 2D spline interpolation [33]. The experimental result of our implementation is presented in Fig. 1 for the finest level 7, and the result of the previous levels 3 : 6 are displayed in Fig. 2(a)–(d). As it can be seen the method has effectively separated the intensity changes of the two images being registered.

In the second experiment, similarly we apply the technique to a DCE-MRI series of abdominal data which are displayed in Fig. 3 with the parameters $\alpha = 200$, $\beta = 30$, $\epsilon = 50$, $\mu = 1$, and $\lambda = 0$.

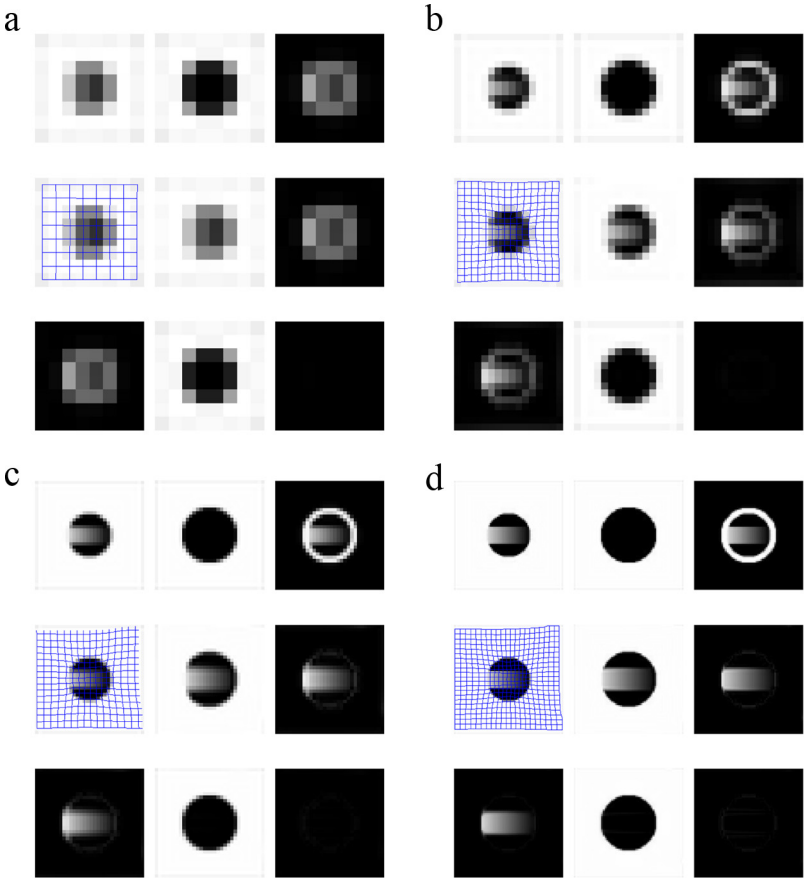

Fig. 2 – Multi-level Gauss–Newton approach to joint image registration and intensity correction of a disk example for levels (a) 3, (b) 4, (c) 5, and (d) 6. The order of displayed images are consistent with images displayed for the last level in Fig. 1.

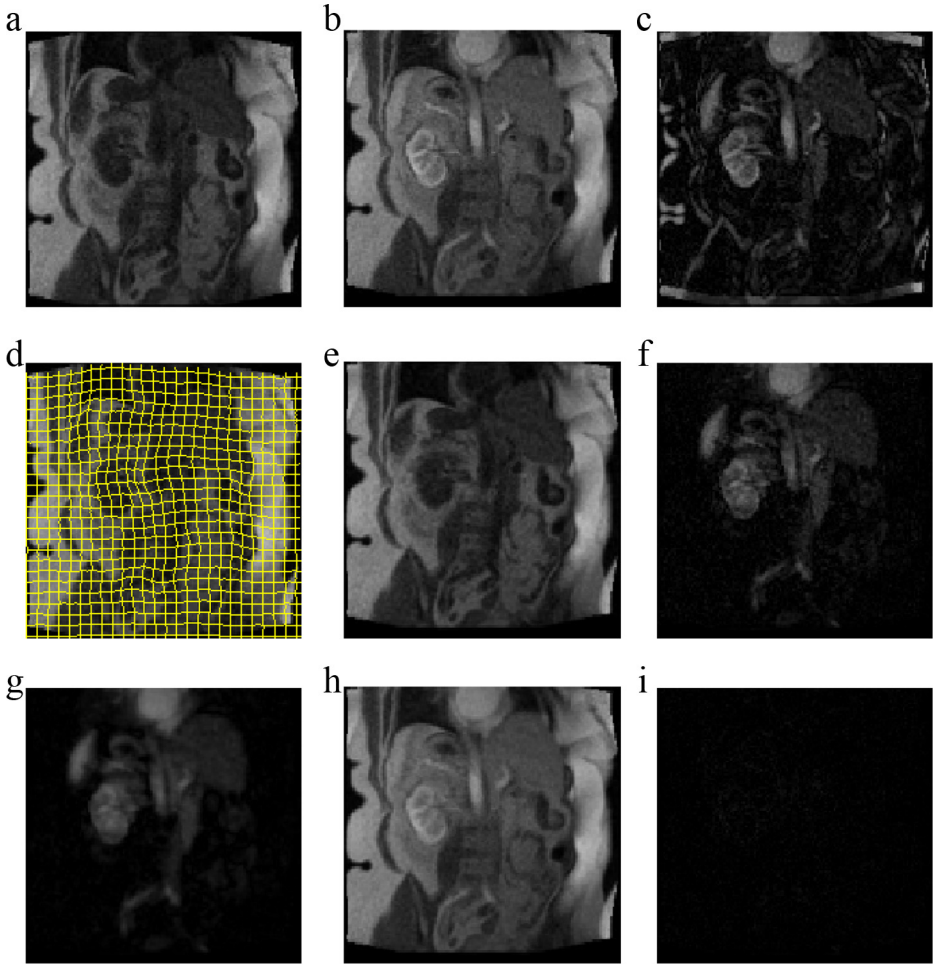

Fig. 3 – Multi-level Gauss–Newton approach to joint image registration and intensity correction applied to a DCE-MRI abdominal data for level 7: (a) Template $T(x)$. (b) Reference $R(x)$. (c) $|T(x) - R(x)|$. (d) Template $T(x)$ and the grid y (e) Transformed template $T(y)$. (f) $|T(y) - R(x)|$. (g) Intensity correction $|w(x)|$. (h) $T(y) + w(x)$. (i) $|T(y) + w(x) - R(x)|$.

Similarly the method has captured and corrected the intensity changes of the two images.

In each experiment, it was required to set five main parameters α, β, ϵ, μ, and λ. The two parameters μ and λ also known as lame parameters were assigned values comparable to the values introduced in [33], i.e. $\mu = 1$ and $\lambda = 0$. We chose values for ϵ in a range that is 10 to 100 folds smaller than $\|\nabla w(x)\|^2$ over most values of $x \in \Omega$ as defined in Equation (4). Finally, we needed to tune the parameters α and β. By choosing a large value of α compared to β, the method tends to associate the intensity differences of $\mathcal{R}$ and $\mathcal{T}$ to the intensity correction term w, while choosing a small value of α compared to β forces the method to correct the intensities by transforming the template image $\mathcal{T}$.

6. Validation

Proper validation involves the registration of a set of contrast-enhanced images with motion characteristics that are described by some known transformation. If invertible, the inverse of this transformation can be compared to the transformation output by image registration in order to evaluate accuracy. To provide for this, we apply a known invertible transformation to simulate motion in a motionless clinical DCE-MRI scan of the abdomen.

In practice, there is always some motion present in DCE-MRI scans. Consequently, a motionless dataset must be constructed. A previously described method [26] using an alternative registration technique and principal components reconstruction was used to create a motionless dataset with realistic contrast enhancement patterns. Though particularly effective at producing a motionless dataset, this technique removes some image information and is therefore not suitable for motion correction outside of a simulation context.

Similar to [26], motion is simulated by modeling the diaphragm as a half sinusoid with temporally varying amplitude. The SI displacement of a point in the image volume with LR coordinate x at time t is given by

$$\Delta SI(x, t) = -\Delta SI_{\max} |\sin(\pi t / t_b)| \sin(\pi x / x_{\max}) \quad (15)$$

where $\Delta SI_{\max}$ corresponds to the maximum SI displacement. $\Delta SI_{\max} = 20$ mm was selected as it falls within the range of typical maximum SI displacements observed for abdominal

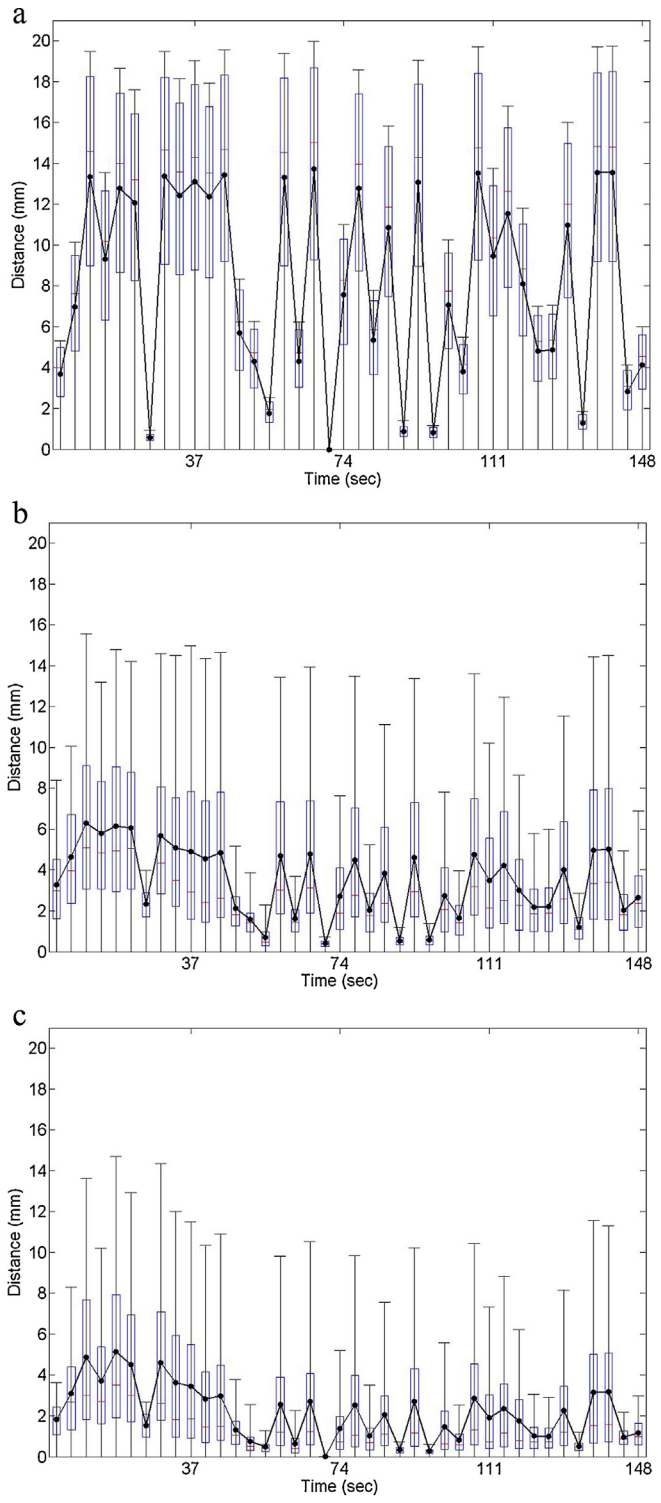

Fig. 4 – Distributions of the distance of pixels from their location in the motionless dataset (a) Before registration. (b) After NGF registration (c) After the proposed registration. In all figures the first 40 time-points are shown. Box plots encompass the 25–75th quartiles and whiskers encompass 97.5 of all values. The average is denoted by a black line.

organs [1]. x_{max} is the maximum LR extent of the patient, and the respiration rate is given by $1/t_b$. The respiration rate is sampled from a Gaussian distribution upon each new breath and centered about the average respiratory rate of humans, 15 breaths/min ($\sigma = 2$ breaths/min) [3]. A small rotation about the centre of the images is added, where the angle of rotation at time t is given by,

$$\theta(t) = |\sin(\pi t/t_b)|\theta_{max} \quad (16)$$

where $\theta_{max} = 1^\circ$ is the maximum permitted rotation. Since the applied transformation and is known, the distance of pixels from their location in the motionless dataset can be determined (Fig. 4(a)). The average magnitude of these distances was 8.2 mm ($\sigma = 4.7$ mm). Fig. 4(a) contains the information for the first 40 simulated time-points where the consecutive time-points are 3.7 s apart. In addition, the physical size of the data was $481 \times 481\,mm^2$.

The dataset with simulated motion was registered to a single reference image within the motionless dataset using the proposed method. Namely, the 19th image in the sequence, the element right before 74 s displayed on Fig. 4(a) has been used as the reference. In addition we compare our results with the an scheme based on the novel normalized gradient field (NGF) dissimilarity measure which has been shown to be effective in registration of images with different intensities along with the elastic regularization scheme [33].

The NGF dissimilarity measure is a reasonable choice because it deals with gradients, rather than intensities. Therefore it is particularly well-suited to contrast-enhanced dataset registration where intensities change but many edges are preserved. In addition, choosing NGF yields computationally efficient registration algorithms. This suggests that the NGF-scheme seems to be a suitable choice for our comparison.

The parameters for both the NGF and the proposed schemes were tuned to yield the most accurate registration results with respect to the motion-less data set. Following the registration experiments, the NGF-based registration and the proposed method reduced the distance of pixels from their location in the motionless dataset from 8.2 mm ($\sigma = 4.7$ mm) to 3.5 mm ($\sigma = 1.8$ mm) and 2.1 mm ($\sigma = 1.4$ mm), respectively, (Fig. 4(b and c)).

The measured quantities suggest that the proposed scheme not only is capable of correcting the intensities but also outperforms the registration accuracy of the NGF-based scheme. This can be associated to the fact that the proposed joint registration and intensity correction model is more physically motivated. In addition, the complexity of computations for both schemes is essentially identical and the run-time for both algorithms is roughly equivalent.

7. Discussion and concluding remarks

The goal of this research was to overcome the limitations of current registration techniques and to design a new rigorous mathematical model capable of a combined treatment of intensity changes and motion artefacts in an efficient numerical scheme. We specifically employed a multi-level

Gauss–Newton optimization scheme which has been proven to be very efficient for image registration [33].

We validated our method using real and simulated data and quantitatively analyzed the registration accuracy of our approach. Our approach performed a more accurate registration compared to the NGF-based registration on the simulated dataset.

Our simulation study used a relatively simple model of displacement due to respiration and this was found to produce displacements that were visually very similar to those observed in real data. We therefore felt it was not necessary to use a more complex biomechanical simulation using the finite element method (FEM).

In general, the problem of choosing appropriate set of registration parameters can be a challenging task. Here we have manually selected the parameters and have varied the parameters to yield reasonable results.

It should be noted that, our experiments are based on 2D datasets. Extension of the experiments to 3D may seem trivial, however, implementation of matrix-free operations may be essential to guarantee minimal use of memory and processing power for large datasets.

Other related methods such as trust-region, and in particular ℓ-BFGS methods [37] may also be explored. In addition, the performance of pre-conditioned conjugate gradient [22], MinRes [38], and multi-grid schemes [4,47] can be evaluated in this context. Furthermore, for the specific case of TV-norm based homogenization, more recent approaches such as Bregman iteration [44] can be investigated. Regarding the multi-level implementation, more recent work that aims to reduce work load even further [16,17] can also be investigated that represents the problem on an adaptive sparse grid and refines only where necessary.

Acknowledgments

This research was supported in part by the Canadian Breast Cancer Foundation (CBCF). This work was also supported by the Canadian Institutes of Health Research (CIHR). The authors would like to thank Dr. Jan Modersitzki, University of Lübeck, Germany, for his valuable comments in the preparation of this work.

REFERENCES

[1] B. Bussels, L. Goethals, M. Feron, D. Bielen, S. Dymarkowski, P. Suetens, K. Haustermans, Respiration-induced movement of the upper abdominal organs: a pitfall for the three dimensional conformal radiation treatment of pancreatic cancer, Radiotherapy & Oncology 68 (2003) 69–74.

[2] D.C. Barber, D.R. Hose, Automatic segmentation of medical images using image registration: diagnostic and simulation applications, Journal of Medical Engineering and Technology 29 (2) (2005 03) 53–63.

[3] B. Beckett, Illustrated Human and Social Biology, Oxford University Press, Oxford, 1999.

[4] W.L. Briggs, V.E. Henson, S.F. McCormick, A Multigrid Tutorial, 2 ed., SIAM, Philadelphia, 2000.

[5] L.G. Brown, A survey of image registration techniques, ACM Computing Surveys 24 (4) (1992) 325–376.

[6] G.A. Buonaccorsi, J.P.B. O'Connor, A. Caunce, C. Roberts, S. Cheung, Y. Watson, K. Davies, L. Hope, A. Jackson, G.C. Jayson, G.J.M. Parker, Tracer kinetic model-driven registration for dynamic contrast-enhanced MRI time-series data, Magnetic Resonance in Medicine 58 (5) (2007 Nov) 1010–1019.

[8] M. Ebrahimi, A.L. Martel, A general PDE-framework for registration of contrast enhanced images., in: D. Hawkes, D. Rueckert, G.Z. Yang (Eds.), Lecture Notes in Computer Science, Proceedings of Medical Image Computing and Computer Assisted Intervention (MICCAI), vol. 5761, Springer-Verlag, London, UK, 2009, pp. 811–819.

[9] M. Ebrahimi, A.L. Martel, Image registration under varying illumination: Hyper-demons algorithm., in: D. Cremers, Y. Boykov, A. Blake, F.R. Schmidt (Eds.), Lecture Notes in Computer Science, Proceedings of Energy Minimization Methods in Computer Vision and Pattern Recognition (EMMCVPR), vol. 5681, Springer-Verlag, Bonn, Germany, 2009, pp. 303–316.

[10] B. Fischer, J. Modersitzki, Ill-posed medicine - an introduction to image registration, Inverse Problems 24 (2008) 1–19.

[13] M.A. Gennert, S. Negahdaripour, Relaxing the brightness constancy assumption in computing optical flow. 62 Computers, Control and Information Theory AIMEMO975; ADA1874379 MIT, June, 1987.

[14] C. Glasbey, A review of image warping methods, Journal of Applied Statistics 25 (1998) 155–171.

[15] A. Ardeshir, Goshtasby, 2-D and 3-D Image Registration, Wiley Press, New York, 2005.

[16] E. Haber, S. Heldmann, J. Modersitzki, An octree method for parametric image registration, SIAM Journal on Scientific Computing 29 (5) (2007) 2008–2023, http://dx.doi.org/10.1137/060662605.

[17] E. Haber, S. Heldmann, J. Modersitzki, Adaptive mesh refinement for nonparametric image registration, SIAM Journal on Scientific Computing 30 (6) (2008) 3012–3027, DOI: 10.1137/070687724.

[18] E. Haber, J. Modersitzki, Numerical methods for volume preserving image registration, Inverse Problems, Institute of Physics Publishing 20 (5) (2004) 1621–1638.

[19] E. Haber, J. Modersitzki, Image registration with a guaranteed displacement regularity, IJCV 1 (2006), http://dx.doi.org/10.1007/s11263-006-8984-4.

[20] E. Haber, J. Modersitzki, A multilevel method for image registration, SIAM: SIAM Journal on Scientific Computing 27 (5) (2006) 1594–1607.

[21] J. Hajnal, D. Hawkes, D. Hill, Medical Image Registration, CRC Press, 2001.

[22] M.R. Hestenes, E. Stiefel, Methods of conjugate gradients for solving linear systems, Journal of Research of the National Bureau of Standards 49 (1952) 409–436.

[24] D.L.G. Hill, P.G. Batchelor, M. Holden, D.J. Hawkes, Medical image registration, Physics in Medicine and Biology 46 (2001) R1–R45.

[25] B.K.P. Horn, B.G. Schunck, Determining optical flow, Artificial Intelligence 17 (1–3; special volume) (1981), 185–203, 8.

[26] A. Lausch, M. Ebrahimi, A. Martel, Image registration for abdominal dynamic contrast-enhance magnetic resonance images, in: 8th IEEE International Symposium on Biomedical Imaging: From Nano to Macro, 2011, pp. 561–565.

[27] H. Lester, S.R. Arridge, A survey of hierarchical non-linear medical image registration, Pattern Recognition 32 (1999) 129–149.

[29] A.L. Martel, D.B. Plewes, M.S. Froh, K.K. Brock, D.C. Barber, Evaluating an optical-flow-based registration algorithm for contrast-enhanced magnetic resonance imaging of the breast, Physics in Medicine and Biology 52 (13) (2007) 3803–3816.

[31] A. Melbourne, D. Atkinson, M.J. White, D. Collins, M. Leach, D. Hawkes, Registration of dynamic contrast-enhanced MRI using a progressive principal component registration (PPCR), Physics in Medicine and Biology 52 (17) (2007 Sep 07) 5147–5156.
[32] J. Modersitzki, Numerical Methods for Image Registration, Oxford University Press, Oxford, 2004.
[33] J. Modersitzki, (FAIR) Flexible Algorithms for Image Registration, SIAM, 2009.
[34] J. Modersitzki, N. Papenberg, A Unified Approach to Registration and Intensity Correction (ric). Unavailable Preprint A-06-05, Results Presented on Pages 80–84, 2008 http://www.siam.org/meetings/op08/Modersitzki.pdf
[35] J. Modersitzki, S. Wirtz, Combining homogenization and registration, in: J.P.W. Pluim, et al. (Eds.), Biomedical Image Registration: Third International Workshop, WBIR 2006, LNCS, Springer, 2006, pp. 257–263.
[36] S. Negahdaripour, C.H. Yu, A generalized brightness change model for computing optical flow, in: 1993 IEEE 4th International Conference on Computer Vision, Publ by IEEE, 1993, pp. 2–11.
[37] J. Nocedal, S.J. Wright, Numerical Optimization, 2nd ed., Springer, 2006.
[38] C.C. Paige, M.A. Saunders, Solution of sparse indefinite systems of linear equations, SIAM Journal on Numerical Analysis 12 (4) (1975) 617–629.
[39] J.P.W. Pluim, J.B.A. Maintz, M.A. Viergever, Mutual-information-based registration of medical images: a survey, IEEE TMI 22 (1999) 986–1004.
[40] K. Rohr, Landmark-based Image Analysis. Computational Imaging and Vision, Kluwer Academic Publishers, Dordrecht, 2001.
[41] L.I. Rudin, S. Osher, E. Fatemi, Nonlinear total variation based noise removal algorithms, Physica D: Nonlinear Phenomena 60 (1-4) (1992) 259–268.
[42] O. Scherzer, Mathematical Models for Registration and Applications to Medical Imaging, Springer, New York, 2006.
[44] X.-C. Tai, C. Wu, Augmented Lagrangian method, dual methods and split Bregman iteration for rof model., in: The 2nd international conference on SSVM, Berlin, Heidelberg, LNCS 5567, 2009, pp. 502–513.
[45] J. Thirion, Non-rigid matching using demons, in: IEEE, Correspondence on Computer Vision and Pattern Recognition, 1996, pp. 245–251.
[47] U. Trottenberg, C. Oosterlee, A. Schüller, Multigrid, Academic Press, 2001.
[49] C.R. Vogel, Computational Methods for Inverse Problems, SIAM, 2002.
[50] J. Weickert, A. Bruhn, T. Brox, N. Papenberg, A survey of variational optic flow methods for small displacement, in Mathematical Models for Registration and Applications to Medial Imaging, Springer, 2005.
[51] T.S. Yoo, Insight into Images: Principles and Practice for Segmentation, Registration, and Image Analysis, AK Peters Ltd., 2004.
[52] Y. Zheng, J. Yu, C. Kambhamettu, S. Englander, M.D. Schnall, D. Shen, De-enhancing the Dynamic Contrast-Enhanced Breast MRI for Robust Registration, vol. 4791, Springer-Verlag, Berlin, MICCAI, 2007.
[53] B. Zitová, J. Flusser, Image registration methods: a survey, Image and Vision Computing 21 (11) (2003) 977–1000.